Title

Conditional Deletion of Sost in MSC-Derived Lineages Identifies Specific Cell-Type Contributions to Bone Mass and B-Cell Development

Journal

Journal of Bone and Mineral Research, 33(10)

ISSN

0884-0431

Authors

Yee, Cristal S
Manilay, Jennifer O
Chang, Jiun C
et al.

Publication Date

2018-10-01

DOI

10.1002/jbmr.3467

Peer reviewed

ORIGINAL ARTICLE

JBMR®

Conditional Deletion of *Sost* in MSC-Derived Lineages Identifies Specific Cell-Type Contributions to Bone Mass and B-Cell Development

Cristal S Yee,[1,2*] Jennifer O Manilay,[2*] Jiun C Chang,[1,2] Nicholas R Hum,[1] Deepa K Murugesh,[1] Jamila Bajwa,[2] Melanie E Mendez,[1,2] Aris E Economides,[3] Daniel J Horan,[4] Alexander G Robling,[4] and Gabriela G Loots[1,2]

[1]Physical and Life Sciences Directorate, Lawrence Livermore National Laboratories, Livermore, CA, USA
[2]Molecular Cell Biology Unit, School of Natural Sciences, University of California-Merced, Merced, CA, USA
[3]Regeneron, Tarrytown, NY, USA
[4]Department of Anatomy and Cell Biology, Indiana University School of Medicine, Indianapolis, IN, USA

ABSTRACT

Sclerostin (Sost) is a negative regulator of bone formation and blocking its function via antibodies has shown great therapeutic promise by increasing both bone mass in humans and animal models. Sclerostin deletion in *Sost* KO mice (*Sost*$^{-/-}$) causes high bone mass (HBM) similar to sclerosteosis patients. *Sost*$^{-/-}$ mice have been shown to display an up to 300% increase in bone volume/total volume (BV/TV), relative to age-matched controls. It has been postulated that the main source of skeletal sclerostin is the osteocyte. To understand the cell-type specific contributions to the HBM phenotype described in *Sost*$^{-/-}$ mice, as well as to address the endocrine and paracrine mode of action of sclerostin, we examined the skeletal phenotypes of conditional *Sost* loss-of-function (*Sost*$^{iCOIN/iCOIN}$) mice with specific deletions in (1) the limb mesenchyme (*Prx1-Cre;* targets osteoprogenitors and their progeny); (2) midstage osteoblasts and their progenitors (*Col1-Cre*); (3) mature osteocytes (*Dmp1-Cre*); and (4) hypertrophic chondrocytes and their progenitors (*ColX-Cre*). All conditional alleles resulted in significant increases in bone mass in trabecular bone in both the femur and lumbar vertebrae, but only *Prx1-Cre* deletion fully recapitulated the amplitude of the HBM phenotype in the appendicular skeleton and the B-cell defect described in the global KO. Despite WT expression of *Sost* in the axial skeleton of *Prx1-Cre* deleted mice, these mice also had a significant increase in bone mass in the vertebrae, but the sclerostin released in circulation by the axial skeleton did not affect bone parameters in the appendicular skeleton. Also, both *Col1* and *Dmp1* deletion resulted in a similar 80% significant increase in trabecular bone mass, but only *Col1* and *Prx1* deletion resulted in a significant increase in cortical thickness. We conclude that several cell types within the *Prx1*-osteoprogenitor-derived lineages contribute significant amounts of sclerostin protein to the paracrine pool of *Sost* in bone. © 2018 The Authors. *Journal of Bone and Mineral Research* Published by Wiley Periodicals, Inc.

KEY WORDS: Sost; SCLEROSTIN; MSC; OSTEOBLAST; OSTEOCYTE; CHONDROCYTE; WnT SIGNALING; WnT

Introduction

Sclerostin (Sost) is a secreted Wnt antagonist that primarily functions to negatively regulate bone formation by preventing the propagation of Wnt signaling through the low-density lipoprotein receptor-related proteins (LRP4/5/6 Wnt coreceptors) in osteoblasts, preosteocytes, and osteocytes.[1,2] Patients carrying homozygous *SOST* null mutations (sclerosteosis) display generalized high bone mass (HBM),[3,4] a phenotype that is recapitulated in *Sost* KO mice (*Sost*$^{-/-}$).[5,6] Conversely, overexpression of *SOST* in transgenic mice (*SOST*^{tg}) results in osteopenia.[7] Shortly after the gene responsible for sclerosteosis was cloned, *SOST* transcripts were reported in bone, BM, cartilage, kidney, liver, lung, heart, and pancreas[3,4]; however, histological examination determined that the osteocytes within cortical and trabecular bone were a dominant source of sclerostin.[8,9] These observations support the hypothesis that the HBM phenotype in both patients and mice is based on a sclerostin deficiency in osteocytes, and that sclerostin acts in a paracrine manner.[10]

Recent reports have provided new evidence that sclerostin may also act in an endocrine manner. Sclerostin serum levels were found to correlate with bone phenotypes: Several groups have shown that serum sclerostin levels are elevated in

Received in original form October 10, 2017; revised form April 26, 2018; accepted April 28, 2018. Accepted manuscript online May 11, 2018.
Address correspondence to: Gabriela G. Loots, Biology and Biotechnology Division, Lawrence Livermore National Laboratory, 7000 East Avenue, L-452, Livermore, CA 94550. E-mail: loots1@llnl.gov
*Drs. Yee and Manilay contributed equally to this work.
Additional Supporting Information may be found in the online version of this article.
Journal of Bone and Mineral Research, Vol. xx, No. xx, Month 2018, pp 1–12
DOI: 10.1002/jbmr.3467

postmenopausal women compared with premenopausal women.[11,12] Estrogen treatment administered to postmenopausal women significantly decreased serum sclerostin and mRNA levels in bone biopsies compared with untreated postmenopausal women,[11–13] suggesting that estrogen may function to inhibit *Sost* expression/production.[12,14] Similarly, an increase in SOST serum levels was documented for aging men and women.[12]

Sclerostin serum levels are affected by age, sex, hormone, and disease status, suggesting that sclerostin serum levels could impact bone physiology. Osteocytes are the likely source of most of the circulating sclerostin found in serum. Thus, all of the above-mentioned sclerostin-modulating factors could control sclerostin transcriptionally or posttranscriptionally in bone. Another unresolved issue is whether bone-associated cell types other than osteocytes also contribute to the sclerostin protein pool locally and systemically, including osteoblasts, osteoclasts, bone-lining cells, mesenchymal stem cells, or other progenitors along the osteoblastic- and chondrogenic-lineages. To understand the cell-type specific contributions to the HBM phenotype described in $Sost^{-/-}$ mice and to address the endocrine and paracrine mode of action of sclerostin, we examined the skeletal phenotypes of conditional *Sost* loss-of-function ($Sost^{iCOIN/iCOIN}$) mice with specific deletions in (1) the limb mesenchyme (*Prx1-Cre*-driven recombination), which targets osteoprogenitors and their progeny; (2) midstage osteoblasts and their progenitors (*Col2.3-Cre*-driven recombination); (3) early-stage osteocytes (*Dmp1-Cre*-driven recombination); and (4) hypertrophic chondrocytes and their progenitors (*ColX-Cre*).

We were particularly interested in determining whether any of these mice phenocopy the global *Sost* deletion. Here we show that conditional deletion of *Sost* in *Prx1*-expressing cells recapitulates the global high-bone-mass phenotype of $Sost^{-/-}$, resulting in ~250% more bone in the femur. In contrast, both *Col1*- and *Dmp1*-specific deletions of *Sost* induced a significant, but milder increase in bone formation, only 30% that of $Sost^{-/-}$, or ~80% more bone than WT controls. The vertebrae of *Prx1-Cre*–deleted *Sost* mice also displayed a significant 50% increase in bone mass, suggesting that limb–bone-derived sclerostin contributes significantly to the serum pool of sclerostin that normally suppresses bone formation in the spine. Moreover, the sclerostin produced in the axial skeleton (ie, in the skeletal tissues that avoid *Prx1-Cre*–mediated recombination) is too dilute in the circulation to impair bone formation rates in the appendicular skeleton, where the *Sost* gene is recombined.

In addition, the relationships and interactions between the diverse cell types within the bone and their reciprocal effects on each other's cell fate decisions have become a focus of intense research, with clinical applications to improve bone fracture healing, prevent age-related bone loss and immune deficiencies. A significant knowledge gap exists as to the contribution of different osteolineage cells to the differentiation, proliferation, and long-term survival of B lymphocytes in the BM. In global sclerostin KO ($Sost^{-/-}$) mice, we previously uncovered a cell-extrinsic requirement for sclerostin on B-lymphocyte development.[15] Similar to mice with global *Sost* deletion, the total BM cellularity in the femurs and tibiae was significantly reduced when *Sost* was deleted from *Prx1*-expressing cells. However, B-lymphocyte development was differentially affected by *Sost* deletion in the *Prx1*-, *Col1*-, and *Dmp1*-expressing cells, suggesting that a specific population of sclerostin-expressing cells in the bone influences B-cell development and function.

Materials and Methods

Experimental animals

Mice with *C57Bl/6* background were used in this study. *Sost* conditional KO ($Sost^{iCOIN/iCOIN}$) mice were generated by inserting an inverted GFP cassette, flanked by lox66 and lox71 sequences, in the intron of the *Sost* gene as previously described.[16] Female mice with Cre under the *Prx1* promoter [B6.Cg-Tg(Prrx1-cre)1Cjt/J], *Col1* promoter [Tg(Col1a1-cre)2Bek], *Dmp1* promoter [B6N.FVB-Tg(Dmp1-cre)1Jqfe/BwdJ], or *ColX* promoter [Tg(Col10a1-cre)1421Vdm] were mated to $Sost^{iCOIN/iCOIN}$ male mice to generate conditional mutations in $Sost^{iCOIN/iCOIN}$; *Prx1-Cre*, $Sost^{iCOIN/iCOIN}$; *Col1-Cre*, $Sost^{iCOIN/iCOIN}$; *Dmp1-Cre* and $Sost^{iCOIN/iCOIN}$; *ColX-Cre* mice, respectively. Genotyping was completed by PCR. At 16 weeks of age, bones were dissected and processed for μCT, RNA, histology, and immunofluorescence (IF). All animal work was IACUC-approved and performed at Lawrence Livermore National Laboratory or UC Merced in facilities accredited by the Association for Assessment and Accreditation of Laboratory Animal Care International.

Immunofluorescent staining

Femur and lumbar vertebrae were collected at 16 weeks of age; they were fixed, dehydrated, embedded, and sectioned as previously described.[5] For IF, trypsin/EDTA was used for antigen retrieval for 25 min at 37°C. Primary antibodies: anti-SOST (R&D, AF1589), anti-GFP (Abcam,Cambridge, MA, USA; ab13970), and anti-activated β-catenin (Millipore, Billerica, MA, USA) were used and incubated overnight at room temperature as previously described.[17] Negative control slides were incubated with secondary antibody only. Stained slides were mounted with Prolong Gold with 4,6-diamidino-2-phenylindole (DAPI; Molecular Probes, Eugene, OR, USA). ImagePro Plus V7.0 software (Media Cybernetics, Rockville, MD, USA) and a QIClick CCD camera (QImaging, Surrey, BC, Canada) were used for imaging and photo editing.

Micro-computed tomography

Fourth lumbar vertebrae and whole femora were collected and fixed for 48 hours in 10% neutral buffered formalin, then stored in 70% ethanol at 4°C until scanning. The entire vertebra and the distal 60% of the femur were scanned on a Scanco μCT-35 specimen scanner (Scanco Medical AG, Brüttisellen, Switzerland) using 60 kVp, 180 mA, 750-ms integration time, and 10-μm voxel size.[18] The entire cancellous region of the lumbar vertebra within 100 um of the endplates was isolated by manual analysis and included in the analysis. For the distal femur metaphysis, a 2-mm region of secondary spongiosa was isolated by manual analysis. The region of interest began 1-mm proximal to the distal growth plate and extended proximally for 2 mm. Prior to scanning, the total length of each femur was measured with digital calipers; these measurements were used to identify the mid-diaphysis slice in each femur CT scan by taking into account slice thickness (10 μm) and counting up in slices from the distal tip of the condyles until the calculated midshaft was reached. The central 20 slices at midshaft were analyzed for cortical properties.

Western blot and ELISA

Femur and lumbar vertebrae were collected from 12- to 16-week-old age-matched mice, frozen in liquid nitrogen, and

stored at −80 °C until extraction. The bones were homogenized in 500 μL of radioimmunoprecipitation assay buffer with an appropriate volume of protease inhibitor cocktail (Sigma-Aldrich, St. Louis, MO, USA) at 1 mL/20*g* tissue, then incubated on ice for 20 min prior to centrifugation at 18,000*g* for 20 min at 4 °C. The protein lysate supernatant was then quantified using BCA assay (Pierce, Rockford, IL, USA) and stored at −80 °C. SDS-PAGE was performed with equal quantities of total protein per sample on NuPAGE protein gels (Thermo Fisher Scientific, Rockford, IL, USA). Protein was then blotted onto a PVDF membrane (LI-COR Biosciences, Lincoln, NE, USA) for Western blot analysis. Membranes were probed with primary antibodies specific for Sost (AF1589; R&D Systems, Minneapolis, MN, USA) and β-actin (926-42210, LI-COR Biosciences) followed by IRDye 800CW donkey anti-goat and IRDye 680RD donkey anti-rabbit secondary antibodies (LI-COR Biosciences). Membranes were then imaged using an Odyssey FC imaging system (LI-COR Biosciences). Mouse sclerostin (41-SCLMS-EO1; ALPCO, Salem, NH, USA), Rankl (R&D Systems Cat#MTR00), and Ctx-1 ELISA kits (RatLaps EIA CTX-1 Cat# AC-06F1; Immunodiagnostics, Fountain Hills, AZ) were used according to the manufacturer's instructions (1:10 dilution for sclerostin and 1:1 dilution for Rankl and Ctx-1) to measure serum levels as previously described ($N = 3$ to 4 per group).[19]

Bone marrow harvests

Mice were euthanized by CO_2 inhalation followed by cervical dislocation. Whole legs were dissected and muscles were removed. Bones were crushed with a mortar and pestle in medium 199 containing 2% fetal calf serum (M199+) to release the BM. BM cells were rinsed away from the bone chips with PBS and collected into 15-mL conical tubes, resuspended by trituration and filtered through 70-μ nylon mesh squares into sterile tubes. Cells were next washed with M199+ and centrifuged at 1500 rpm at 4°C for 5 min, after which cell pellets were resuspended and treated with ACK lysis buffer to remove erythrocytes. The ACK-treated cells were washed and resuspended in M199+; total cell counts were obtained using a hemocytometer and trypan blue staining to exclude dead cells.

Analysis of hematopoietic cell lineages by flow cytometry

The following antibodies were purchased from eBioscience (Santa Clara, CA, USA) or Biolegend (San Diego, CA, USA): CD45- (30F11-) FITC, CD19- (6D5-) PE, GR1- (RB6-8C3-) PECy7, CD3- (145-2C11-) APC, CD11b- (M1/70-) biotin, purified FcBlock CD16/32 (90), CD25- (PC61-) FITC, BP1- (Ly51/6C3-) PE, B220- (RA3-6B2-) PECy7, CD117- (2B8-) APC, Rat IgG2a-PE, kappa isotype control, CD19- (6D5-) FITC, CD43- (1B11-) PE, IgM- (eb121-15F9-) eFluor450, IgM- (RMM01-) Brilliant Violet (BV) 421, and IgD- (11-26c.2a-) BV510. Per sample, 1 to 2 $\times 10^6$ cells were stained in 96-well V-bottom plates (Nunc, Inc., Rochester, NY, USA) with their designated antibody cocktail and incubated for at least 15 min at 4 °C before washing with FACS buffer and centrifuging at 2000 rpm at 4 °C for 3 min. Supernatants were removed from the plates and cells incubated with streptavidin-Pacific blue to develop biotinylated CD11b-stained cells when required. Cell viability was assessed using DAPI or propidium iodide (PI) solution at a final concentration of 0.2 μg/mL. Cells were acquired on a Becton Dickinson LSR II (Becton Dickinson, Franklin Lakes, NJ, USA) and flow cytometric analysis was performed using FlowJo software (FlowJo, LLC, Ashland, OR, USA).

Statistics

All data were expressed as the mean ± SD. For μCT and flow cytometry results, statistical analysis was done using a Student's *t* test with a two-tailed distribution, with two-sample equal variance (homoscedastic test) and one-way ANOVA with multiple comparisons. For all tests, $p < 0.05$ was considered statistically significant.

Results

Dmp1-Cre deletion pattern most closely recapitulates endogenous *Sost* expression in bone

Conditional deletion of *Sost* from different cell populations allows us to determine cell-specific contributions to bone metabolism and to distinguish local from systemic effects. Using a previously described *Sost* conditional loss-of-function by inversion allele ($Sost^{iCOIN/iCOIN}$),[16] we eliminated *Sost* expression in (1) the limb mesenchyme (*Prx1-Cre*)[20]; (2) osteoblasts (*Col1-Cre*)[21]; and (3) osteocytes (*Dmp1-Cre*).[22] Upon Cre-mediated recombination, the conditional *Sost* allele undergoes premature termination of the endogenous *Sost* transcript, while simultaneously activating enhanced green fluorescent protein (eGFP) in frame with *Sost*, allowing us to track endogenous Sost expression using eGFP in cells that are now sclerostin-deficient.[16] Previously, it has been shown that a mouse of the $Sost^{iCOIN/LacZ}$; $LacZ^{Nanog\text{-}Cre/+}$ genotype has high bone mass (HBM) indistinguishable from the global *Sost* KO allele that replaces the *Sost* gene with the LacZ reporter ($Sost^{LacZ/LacZ}$; and referred to as $Sost^{-/-}$ in this article).[5,16] Because the *iCOIN*-inverted allele allows us to visualize *Sost*-deficient cells through the presence of eGFP, we first compared the eGFP expression in the bones of $Sost^{iCOIN/iCOIN}$; *Prx1-Cre*, $Sost^{iCOIN/iCOIN}$; *Col1-Cre*, $Sost^{iCOIN/iCOIN}$; *Dmp1-Cre* with the endogenous *Sost* expression in the control $Sost^{iCOIN/iCOIN}$ mice.

Cortical bone expression of eGFP was highest in the osteocytes of *Dmp1-Cre*-deleted mice, and punctate expression was also detected in the matrix, suggesting that the Sost-eGFP fusion protein is able to exit the osteocytes (Fig. 1*A–D*). Because eGFP is a membrane-bound version, we speculate that this expression may be due to microvesicles shed by osteocytes. $Sost^{iCOIN/iCOIN}$; *Col1-Cre*-deleted mice displayed the lowest expression levels in cortical osteocytes (Fig. 1*C*), suggesting that only a minority of embryonically labeled *Col1*-positive cell mature into osteocytes. In the trabecular region of the femurs, *Dmp1-Cre* mice also had the greatest expression; the expression was higher than the endogenous Sost expression (Fig. 1*A*, *D*), suggesting that these cells are accumulating higher levels of Sost-eGFP than in the endogenous bone may be caused by retention of eGFP in the membrane (Fig. 1*E–H*). Similar to the cortical bone results, $Sost^{iCOIN/iCOIN}$; *Col1-Cre* mice also expressed eGFP in fewer trabecular osteocytes (Fig. 1*G*). The expression of eGFP in the vertebrae of $Sost^{iCOIN/iCOIN}$; *Col1-Cre* and $Sost^{iCOIN/iCOIN}$; *Dmp1-Cre* was similar to that described above for the femoral trabeculae; however, consistent with its site of Cre recombinase expression, none of the $Sost^{iCOIN/iCOIN}$; *Prx1-Cre* mice express eGFP in the vertebrae (Fig. 1*I–L*). Western blot analysis showed the highest Sost-eGFP and the lowest Sost expression in the $Sost^{iCOIN/iCOIN}$; *Prx1-Cre* femurs (Prx1), whereas no Sost-eGFP was detected in the vertebrae, consistent with the *Prx1-Cre* site of expression in appendicular skeleton (Fig. 1*M*). Sost serum levels were reduced by ~50% in *Prx1-Cre* mice, but no detectable Sost was measured in *Dmp1-Cre* and *Col1-Cre*

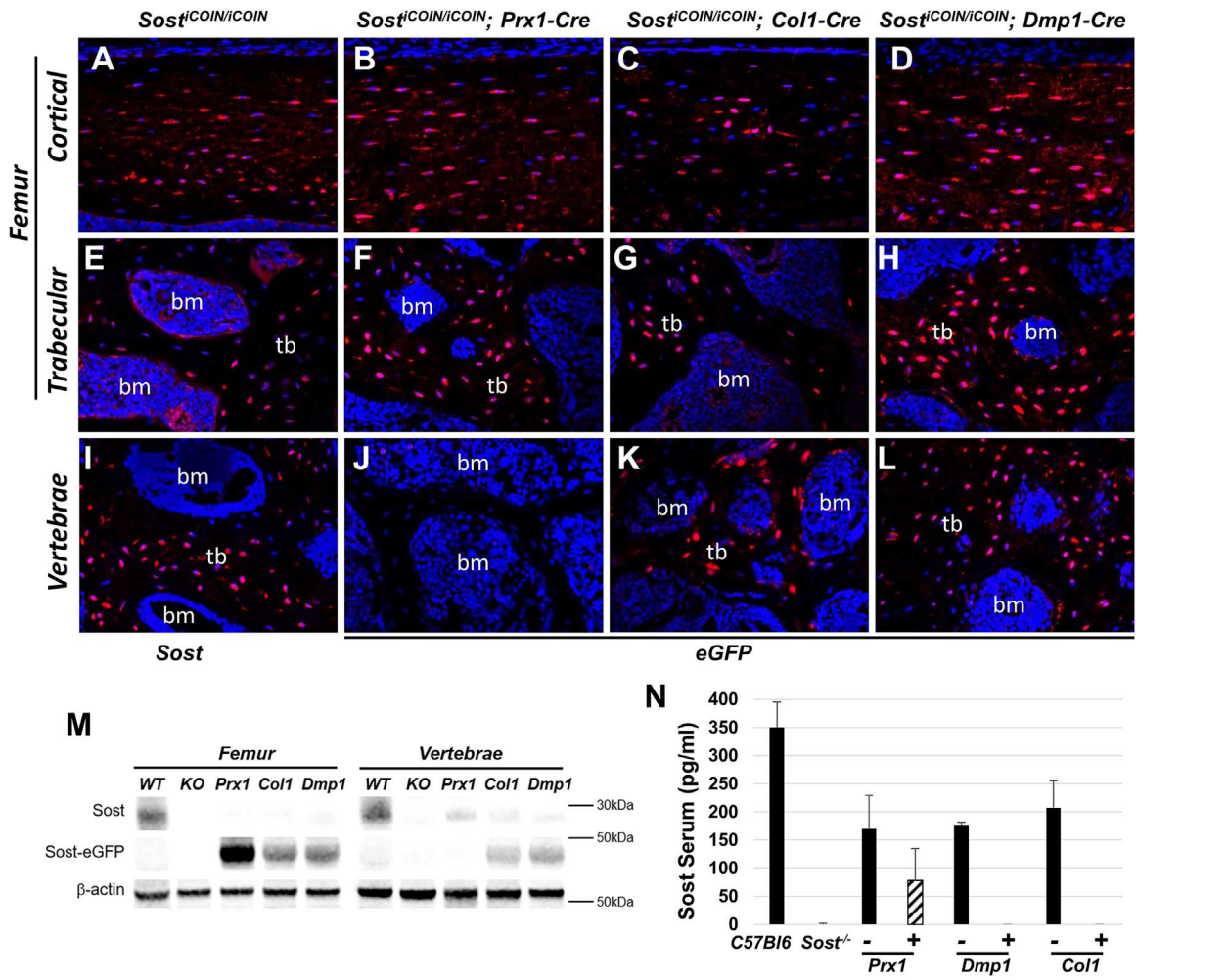

Fig. 1. Evaluating efficiency of *Sost* conditional deletion in bone. Endogenous Sost protein expression in *Sost*$^{iCOIN/iCOIN}$ was visualized in cortical and trabecular bone of the femur (*A, E*) and vertebrae (*I*) by immunohistochemistry and was consistent with previous WT expression of Sost (red) in mice (blue, 4,6-diamidino-2-phenylindole [DAPI]). Cre deletion of Sost allele activates eGFP; Sost-expressing cells and carrying Sost deletion now express a Sost–eGFP fusion protein that is visualized in panels *B*, *C*, *D*, *F*, *G*, *H*, *J*, *K*, *L* in red; blue DAPI. *Prx1-Cre* deletion activated eGFP in *Sost*-deficient cortical (*B*), and trabecular osteocytes (*F*) in the femur, but not in the vertebrae, where Prx1-Cre is not expressed (*J*). *Col1-Cre* deletion activated eGFP in *Sost*-deficient cortical (*C*), and trabecular osteocytes (*G*) in the femur, and also in the osteocytes within the vertebrae (*K*). *Dmp1-Cre* deletion activated eGFP in *Sost*-deficient cortical (*D*), and trabecular osteocytes (*H*) in the femur, and also in the osteocytes within the vertebrae (L). Western blot analysis (M) showed that most of Sost expression was removed in Prx1-, Col1-, and Dmp1-deleted femurs, but Sost expression persisted in the Prx1 vertebrae. eGFP protein expression inversely correlated with the Sost expression (*M*). Sost protein levels in serum (*N*).

mice (Fig. 1*N*). These data suggest that Sost serum levels in *Prx1-Cre* mice are exclusively derived from the axial skeleton.

Dmp1-Cre deletion of Sost does not recapitulate Sost$^{-/-}$ HBM phenotype

Originally, *Sost* was described as an osteocyte specific gene,[23] and although in recent years *Sost* expression has been found in other organs and cell types of the skeleton,[8] osteocytes do express a robust amount of sclerostin (Fig. 1A, E, I); therefore, we anticipated that *Dmp1-Cre* deletion of *Sost* would most closely resemble the HBM phenotype of *Sost*$^{-/-}$ mice. At 16 weeks of age, both *Sost*$^{iCOIN/iCOIN}$*; Col1-Cre* and *Sost*$^{iCOIN/iCOIN}$*; Dmp1-Cre* mice showed a significant increase in femoral BV/TV (Fig. 2*B*, *C*, *E–G*); however, both these values were about one-third of those determined for *Sost*$^{-/-}$ and *Sost*$^{iCOIN/iCOIN}$*; Prx1-Cre* mice, suggesting that both osteoblast- and osteocyte-specific deletion of *Sost* result in the same HBM phenotype (Fig. 2*G*). Vertebral BV/TV was also significantly increased in *Sost*$^{iCOIN/iCOIN}$*; Col1-Cre* and *Sost*$^{iCOIN/iCOIN}$*; Dmp1-Cre* mice by 81% and 88%, respectively, or ~50% of HBM in *Sost*$^{-/-}$ (Fig. 2*G*).

Prx1-Cre deletion recapitulates Sost$^{-/-}$ high bone mass phenotype in the femur

To determine whether conditional ablation of *Sost* in the limb mesenchyme, mature osteoblasts, or osteocytes is sufficient to recapitulate the HBM phenotype observed in the *Sost*$^{-/-}$ mice, we also bred *Sost*$^{iCOIN/iCOIN}$ mice to *Prx1-Cre,* in addition to *Col1-Cre* and *Dmp1-Cre* (Fig. 2*A–D*). All conditional KO mice were indistinguishable in size and weight from their same-sex

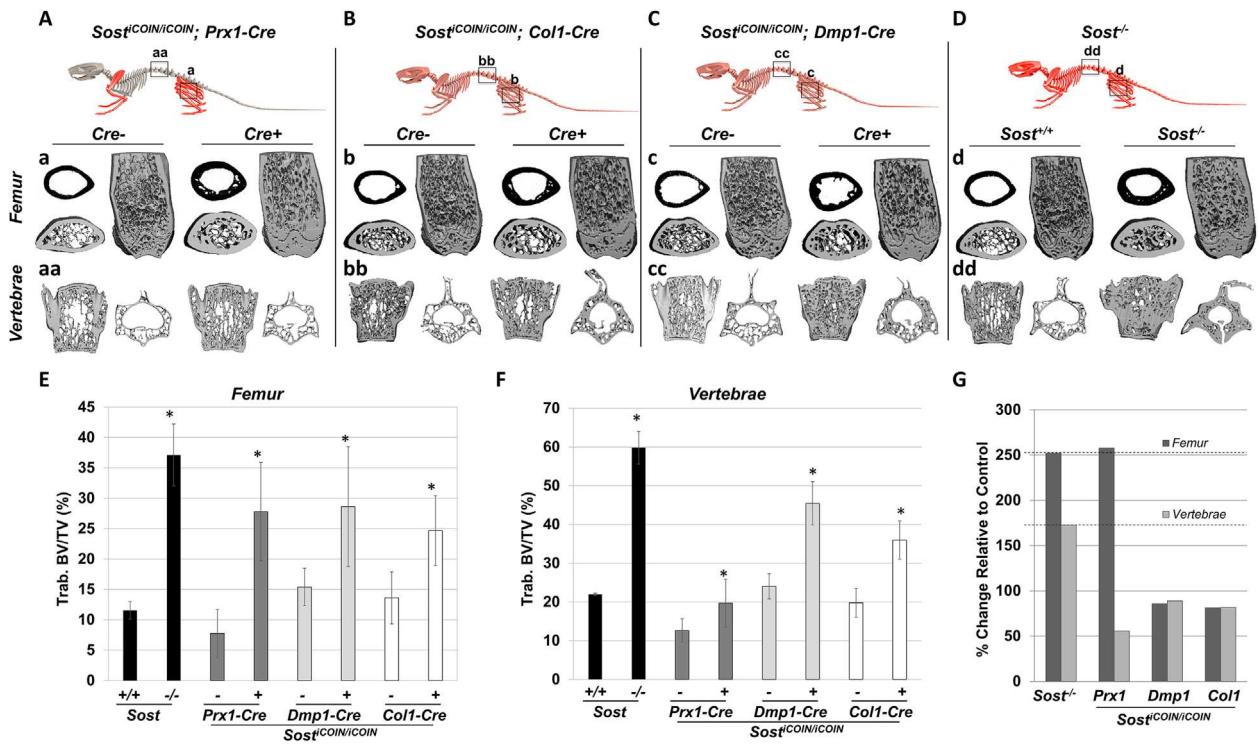

Fig. 2. Comparing skeletal phenotypes of Sost conditional mice to $Sost^{-/-}$ mice. MicroCT analysis of axial and appendicular skeleton of *Prx1-Cre* (*A*), *Col1-Cre* (*B*), *Dmp1-Cre* and $Sost^{-/-}$ (*D*) visually highlights increases in bone mass in both femurs (*a*, *b*, *c*, *d*) and vertebrae (*aa*, *bb*, *cc*, *dd*). *Prx1-Cre* deletes *Sost* in all mesenchymal skin cell-derived cells in the appendicular skeleton only (*A*, red); *Col1-Cre* (*B*), and *Dmp1-Cre* (*C*) delete *Sost* in osteoblast and osteocytes throughout the skeleton; global KO deletes Sost in all cell types of the skeleton (*D*). Quantification of trabecular bone volume/total volume (BV/TV) finds all mice to have a significant increase in both the femoral (*E*) and vertebral (*F*) bone fractions; however, only Prx1-Cre mice had a % change in BV/TV comparable to $Sost^{-/-}$ (*G*). $^{*}p < 0.05$, both by ANOVA and *t* test compared to own Cre negative controls.

Cre-negative control littermates. At 16 weeks of age, a μCT analysis of distal femurs showed that trabecular bone volume fraction (BV/TV) in all conditional KOs was significantly higher than the Cre-negative controls (Fig. 2*A–E*); however, only the $Sost^{iCOIN/iCOIN}$; *Prx1-Cre* mice had a BV/TV increase of 257% (Table 1), a value similar to that of age-matched $Sost^{-/-}$ mice (+221%; Table 2), whereas both $Sost^{iCOIN/iCOIN}$; *Col1-Cre* and $Sost^{iCOIN/iCOIN}$; *Dmp1-Cre* mice had BV/TV increases of 85% and 81%, respectively (Fig. 2*G*; Table 1).

Even though $Sost^{iCOIN/iCOIN}$; *Prx1-Cre* femurs most closely resembled femurs from $Sost^{-/-}$ mice, there were several noted differences. Although $Sost^{-/-}$ did not display a significant increase in trabecular number, with only an 8% increase above WT, $Sost^{iCOIN/iCOIN}$; *Prx1-Cre* femurs had a significant 24.18% increase in trabecular number (Tables, 2 1). Another significant difference was in the cortical values, where $Sost^{iCOIN/iCOIN}$; *Prx1-Cre* femurs did not display significant increases in either cortical bone volume, but had a significant increase in cortical thickness; $Sost^{-/-}$ had a significant 69.98% increase in cortical bone volume and a 31% increase in cortical BV/TV (Tables, 2 1). Furthermore, neither $Sost^{iCOIN/iCOIN}$; *Dmp1-Cre* nor $Sost^{iCOIN/iCOIN}$; *Col1-Cre* had a significant increase in cortical BV/TV despite a significant, but more-modest increase in cortical bone volume (Tables, 2 1). Lastly, cortical bone mineral density was unchanged in all conditional *Sost* mice, whereas $Sost^{-/-}$ mice had a significant 3.21% gain (p value = 0.05) in cortical BMD (Tables, 2 1). Consistent with the bone phenotype, levels of β-catenin were highest in the *Prx1-Cre* cortical and trabecular regions of the femur (Fig. S1).

Prx1-Cre deletion results in increased bone formation in the vertebrae

Prx1-Cre drives Cre recombinase expression in uncommitted mesenchymal cells that contribute to bone, cartilage, muscle, and white and brown adipose tissues of the developing appendicular skeleton. Cre is also expressed in portions of the skull, but absent from other parts of the axial skeleton.[20,24] If *Sost* is retained locally, we anticipated *Prx1-Cre* deletion to cause HBM in the appendicular skeleton and to maintain normal bone mass in the axial skeleton, where *Sost* expression remains unperturbed. Lumbar vertebrae μCT analysis between $Sost^{iCOIN/iCOIN}$; *Prx1-Cre* and age-matched $Sost^{iCOIN/iCOIN}$ control mice uncovered a significant (55%) increase in the BV/TV ratio, suggesting that a lack of *Sost* in the appendicular skeleton positively affects bone formation in the vertebrae (Fig. 2*aa*, *F*, *G*; Table 1). Though trabecular number was not different in $Sost^{iCOIN/iCOIN}$; *Prx1-Cre* than in controls, the trabecular thickness was significantly elevated by 16%. In addition, the trabecular bone mineral content was elevated by 88%, half of the $Sost^{-/-}$ value. Interestingly, neither *Col1-Cre* nor *Dmp1-Cre* deletion of *Sost* resulted in BV/TV increases similar to those measured for $Sost^{-/-}$—displaying an 81% increase and an 88% increase, about half of *Sost* values (Fig. 2*bb*, *cc*, *dd*, *F*, *G*; Tables 1, 2).

Table 1. Bone Phenotyping by microCT

Distal Femur Trabecular and Cortical Compartments

	Prx1-Cre			*Dmp1-Cre*			*Col1-Cre*		
Index	Cre− (N = 6)	Cre+ (N = 5)	% change	Cre− (N = 8)	Cre+ (N = 6)	% change	Cre− (N = 4)	Cre+ (N = 9)	% change
Trab.TV (mm^3)	3.617 ± 0.543	4.472 ± 0.660*	+23.64	4.460 ± 0.686	5.026 ± 0.445	+12.68	3.957 ± 0.537	4.967 ± 0.755*	+25.52
Trab.BV (mm^3)	0.296 ± 0.190	1.278 ± 0.486*	+333.97	0.700 ± 0.215	1.449 ± 0.532*	+106.89	0.554 ± 0.247	1.252 ± 0.433*	+126.15
Trab.BV/TV (%)	0.078 ± 0.039	0.278 ± 0.081*	+257.86	0.154 ± 0.0307	0.286 ± 0.0987*	+85.83	0.136 ± 0.043	0.247 ± 0.058*	+81.25
Trab.Conn.D. ($1/mm^3$)	47.42 ± 38.50	96.71 ± 17.30*	+91.30	102.187 ± 23.29	107.37 ± 13.81	+5.07	77.89 ± 30.64	85.31 ± 31.23	+9.53
Trab.SMI	2.897 ± 0.711	1.049 ± 0.735*	−63.77	2.021 ± 0.511	0.858 ± 0.830*	−57.57	2.188 ± 0.811	1.114 ± 0.572*	−49.08
Trab.N (1/mm)	3.470 ± 0.515	4.309 ± 0.371*	+24.18	4.259 ± 0.237	4.590 ± 0.592	+7.77	3.956 ± 0.407	3.859 ± 0.980	−2.45
Trab.Th (mm)	0.049 ± 0.004	0.080 ± 0.011*	+62.92	0.055 ± 0.0039	0.0729 ± 0.009*	+32.52	0.054 ± 0.004	0.070 ± 0.008*	+29.40
Trab.Sp (mm)	0.291 ± 0.049	0.214 ± 0.024*	−26.45	0.228 ± 0.0153	0.198 ± 0.035*	−13.18	0.248 ± 0.029	0.219 ± 0.019*	−11.90
Trab.BMC ($\mu gHA/cm^3$)	0.270 ± 0.173	1.221 ± 0.475*	+351.83	0.662 ± 0.210	1.396 ± 0.549*	+111.06	0.531 ± 0.243	1.196 ± 0.434*	+125.02
Cort.TV (mm^2)	7.043 ± 0.770	8.670 ± 1.211*	+23.09	7.722 ± 0.863	8.728 ± 0.567*	+13.03	7.519 ± 0.964	9.176 ± 1.214*	+22.05
Cort.BV (mm^2)	2.782 ± 0.523	3.266 ± 1.464	+17.40	2.777 ± 0.219	3.240 ± 0.308*	+16.69	2.783 ± 0.357	3.498 ± 0.468*	+25.69
Cort.BV/TV (%)	0.393 ± 0.041	0.366 ± 0.137	−6.89	0.362 ± 0.029	0.371 ± 0.026	+2.65	0.370 ± 0.007	0.382 ± 0.020	+3.16
Cort. Th (mm)	0.213 ± 0.0124	0.256 ± 0.036*	+20.18	0.229 ± 0.013	0.236 ± 0.033	+0.03	0.217 ± 0.020	0.265 ± 0.022*	+22.11
Cort.BMC ($\mu gHA/cm^3$)	2.909 ± 0.506	3.463 ± 1.529	+19.03	2.990 ± 0.235	3.524 ± 0.356*	+17.86	3.022 ± 0.369	3.800 ± 0.516*	+25.74
Cort.BMD ($\mu gHA/cm^3$)	1.048 ± 0.023	1.065 ± 0.022	+1.56	1.077 ± 0.0114	1.087 ± 0.027	+0.96	1.087 ± 0.010	1.086 ± 0.011	−0.03

Distal Femur Trabecular and Cortical Compartments

	Prx1-Cre			*Dmp1-Cre*			*Col1-Cre*		
Index	Cre− (N = 6)	Cre+ (N = 5)	% change	Cre− (N = 8)	Cre+ (N = 6)	% change	Cre− (N = 4)	Cre+ (N = 9)	% change
Trab.TV (mm^3)	1.710 ± 0.048	1.968 ± 0.204*	+15.13	1.889 ± 0.150	1.772 ± 0.249	−6.20	1.978 ± 1.870	1.786 ± 0.193	−9.75
Trab.BV (mm^3)	0.216 ± 0.053	0.395 ± 0.141*	+82.70	0.464 ± 0.077	0.804 ± 0.149*	+73.46	0.396 ± 0.103	0.646 ± 0.128*	+63.22
Trab.BV/TV (%)	0.127 ± 0.030	0.197 ± 0.062*	+55.61	0.241 ± 0.032	0.454 ± 0.0556*	+88.90	0.198 ± 0.037	0.360 ± 0.050*	+81.69
Trab.Conn.D. ($1/mm^3$)	150.16 ± 45.74	196.39 ± 71.44	+30.79	231.93 ± 29.64	170.98 ± 21.743*	−26.28	217.39 ± 44.74	159.42 ± 23.04*	−26.67
Trab.SMI	1.759 ± 0.287	1.211 ± 0.520*	−31.16	31.62 ± 87.136	−1.225 ± 0.592	−103.87	1.068 ± 0.273	−0.555 ± 0.482*	−151.97
Trab.N (1/mm)	4.233 ± 0.449	4.342 ± 2.007	+2.57	4.591 ± 1.724	6.150 ± 0.389*	+33.95	4.999 ± 0.480	5.402 ± 0.451	+8.071
Trab.Th (mm)	0.040 ± 0.002	0.047 ± 0.006*	+16.36	0.050 ± 0.004	0.074 ± 0.0058	+46.85	0.044 ± 0.004	0.077 ± 0.035	+76.79
Trab.Sp (mm)	0.235 ± 0.028	0.196 ± 0.040	−16.49	0.167 ± 0.053	0.140 ± 0.0127	−16.09	0.192 ± 0.022	0.172 ± 0.017	−10.30
Trab.BMC ($\mu gHA/cm^3$)	0.183 ± 0.047	0.344 ± 0.127*	+88.13	0.408 ± 0.077	0.733 ± 0.144*	+79.70	0.342 ± 0.092	0.566 ± 0.117*	+65.42

Data are from 16-week-old male miceand represent mean ± SD for parameters measured. Trab = trabecular; Cort = cortical; BV = bone volume; TV = total volume; Conn.D. = connectivity density; SMI = structural model index; Trab.N = trabecular number; Trab.Th = trabecular thickness; Trab.Sp = trabecular separation; Cort.Th = cortical thickness; BMC = bone mineral content; BMD = bone mineral density.*p values <0.05 compared to own Cre- control; data from 16-week old males.

Table 2. *Sost*$^{-/-}$ Bone Phenotyping by microCT

Distal Femur Trabecular and Cortical Compartments			
	Sost$^{+/+}$	*Sost*$^{-/-}$	
Index	(N = 5)	(N = 7)	% change
Trab.TV (mm^3)	3.884 ± 0.316	4.316 ± 0.234*	+11.12
Trab.BV (mm^3)	0.452 ± 0.092	1.602 ± 0.242*	+254.57
Trab.BV/TV (%)	0.116 ± 0.015	0.371 ± 0.051*	+221.32
Trab.Conn.D. (1/mm^3)	94.736 ± 20.003	113.01 ± 7.24*	+19.30
Trab.SMI	2.557 ± 0.184	0.257 ± 0.386*	−89.94
Trab.N (1/mm)	4.388 ± 0.229	4.755 ± 0.309	+8.35
Trab.Th (mm)	0.048 ± 0.005	0.090 ± 0.007*	+87.23
Trab.Sp (mm)	0.219 ± 0.013	0.178 ± 0.018*	−18.86
Trab.BMC (μgHA/cm^3)	0.422 ± 0.088	1.506 ± 0.238*	+259.44
Cort.TV (mm^2)	6.887 ± 0.327	8.902 ± 0.362*	+29.23
Cort.BV (mm^2)	2.426 ± 0.094	4.123 ± 0.142*	+69.98
Cort.BV/TV (%)	0.352 ± 0.006	0.463 ± 0.010*	+31.53
Cort.Th (mm)	0.197 ± 0.016	0.321 ± 0.012*	+62.94
Cort.BMC (μgHA/cm^3)	2.596 ± 0.073	4.555 ± 0.139*	+75.46
Cort.BMD (μgHA/cm^3)	1.071 ± 0.015	1.105 ± 0.012*	+3.21
Cancellous (Trabecular) Bone Compartment of the L4 Vertebrae			
	Sost$^{+/+}$	*Sost*$^{-/-}$	
Index	(N = 5)	(N = 7)	% change
Trab.TV (mm^3)	1.694 ± 0.191	1.557 ± 0.193	−8.11
Trab.BV (mm^3)	0.372 ± 0.039	0.934 ± 0.150*	+151.07
Trab.BV/TV (%)	0.220 ± 0.003	0.599 ± 0.042*	+172.49
Trab.Conn.D. (1/mm^3)	243.20 ± 8.512	217.493 ± 35.09	−10.57
Trab.SMI	0.974 ± 0.093	−2.468 ± 0.633*	−353.43
Trab.N (1/mm)	5.383 ± 0.083	7.747 ± 0.314*	+43.93
Trab.Th (mm)	0.044 ± 0.001	0.090 ± 0.008*	+104.73
Trab.Sp (mm)	0.175 ± 0.003	0.104 ± 0.009*	−40.72
Trab.BMC (μgHA/cm^3)	0.330 ± 0.035	0.844 ± 0.142*	+155.46

Data are from 16-week-old male mice and represent mean ± SD for parameters measured. trab = trabecular; cort = cortical; cort.Th = cortical thickness; BV = bone volume; TV = total volume; Conn.D. = connectivity density; SMI = structural model index; Trab.N = trabecular number; Trab. Th = trabecular thickness; Trab.Sp = trabecular separation; BMC = bone mineral content; BMD = bone mineral density.*p values ≤0.05; data from 16-week old males.

Prx1-Cre deletion of Sost results in reduced bone marrow cellularity

To determine which *Sost*-expressing osteolineage cell type is responsible for B-lymphocyte support, we analyzed hematopoietic differentiation in mice lacking *Sost* specifically in osteoprogenitors/mesenchymal stem cells (MSCs) [*Prx1*-Cre], osteoblasts [*Col1a*-Cre], and osteocytes [*Dmp1*-Cre]. Similar to the global *Sost*$^{-/-}$ mouse, *Sost*$^{iCOIN/iCOIN}$*; Prx1-Cre* mice displayed a significant reduction in total BM cellularity; however, deletion of *Sost* in osteoblasts and osteocytes had no effect (Fig. 3*B*). We further examined the frequency (%) and absolute number of total CD19+ B cells, and observed that the percentage of CD19+ cells was slightly reduced when *Sost* was deleted in osteoblasts and osteocytes (Fig. 3*A*, *C*), but the absolute numbers of CD19+ cells were significantly reduced in the *Sost*$^{iCOIN/iCOIN}$*; Prx1-Cre and Sost*$^{iCOIN/iCOIN}$*; Col1-Cre* mice only (Fig. 3*D*).

The CD19+ B cell population in the BM contains a heterogeneous mixture of B-cell progenitors, developing B cells, and mature B cells, which can be distinguished by expression of B220 and diminishing levels of CD43 (Figs. 4*A*, S2*A*).[24] B220+ CD43^{high} cells are B-cell progenitors with low expression of surface IgM and IgD. The B220+ CD43-intermediate (B220+ CD43^{int}) population begins to express surface IgM, and coexpression of IgD can be observed as cells progress to the B220+ CD43^{low} population. Finally, the B220+ CD43-negative (B220+ CD43^{neg}) population is the most mature B-cell population, displaying high levels of IgM and IgD. To determine if the four specific B-cell stages and if their transitions from one stage to the next were differentially affected by *Sost* deletion in specific osteolineage cell types, we enumerated the percentage and absolute numbers of B cells within each B220/CD43 subset, and their expression of IgM and IgD receptors in the conditional *Sost* KO mouse strains. In the global *Sost* KO, a developmental block beginning at the pre-B stage (similar to Hardy Fractions B and C[24]) and all committed B-cell stages were observed[15] with changes in both frequency and cell number. Our analysis of the *Sost*$^{iCOIN/iCOIN}$*; Prx1-Cre* BM showed an increase in the percentage of phenotypically mature B220+ CD43^{neg} cells compared with no Cre controls (Fig. 4*B*). In contrast, the percentage of B220+ CD43^{neg} cells was significantly decreased in the *Sost*$^{iCOIN/iCOIN}$*; Dmp1-Cre* BM. This suggested that deletion of *Sost* in the MSCs resulted in expansion of mature B cells, whereas deletion of *Sost* in the osteocytes resulted in fewer mature B cells. However, the absolute numbers of B220+ CD43^{neg} cells were not affected (Fig. S3). Mature B cells should express high

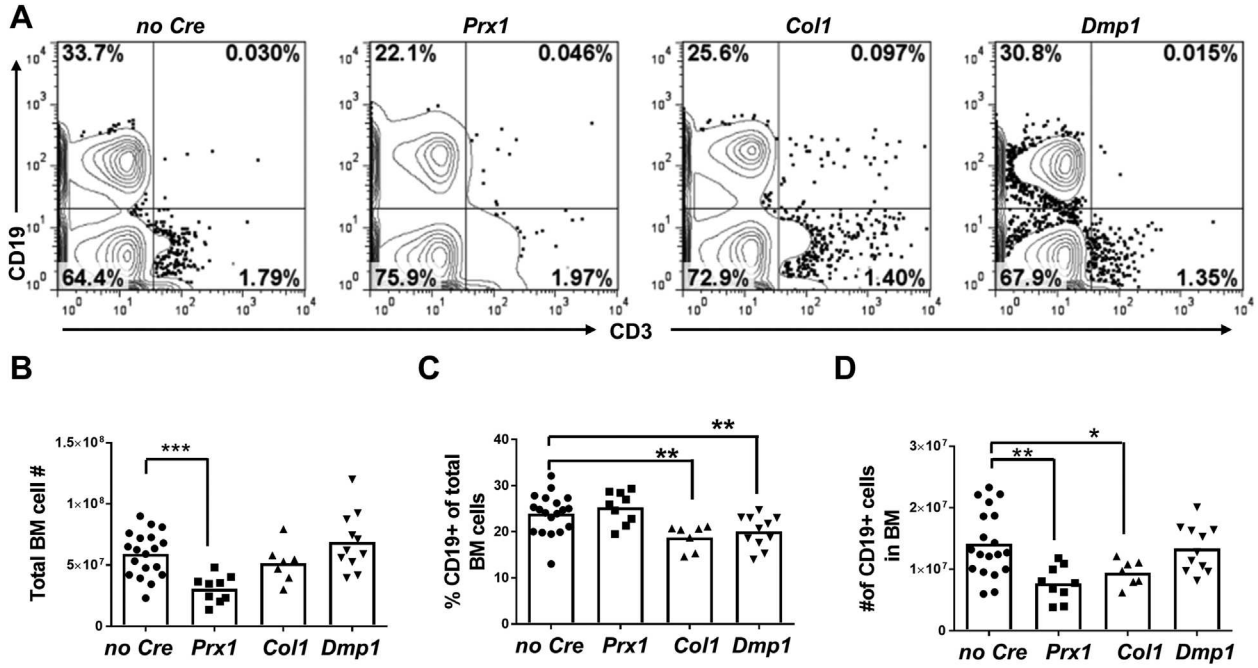

Fig. 3. BM cellularity and lymphocyte frequencies and cell numbers are differentially affected by the absence of Sost in specific osteolineage cell types. Representative flow cytometry plots of CD19 (B-cell) and CD3 (T-cell) lineages in the BM of no-Cre control and conditional *Sost* KO mice (*A*), total BM cellularity (*B*), frequencies of CD19+ cells out of total BM cells (*C*), absolute numbers of CD19+ B cells in BM (*D*). $^{*}p < 0.05$, $^{**}p < 0.01$, $^{***}p < 0.001$ both by ANOVA and *t* test, except in *B*, where comparison of control versus *Prx1-Cre* by ANOVA showed $p < 0.01$, and *C*, where comparison of control versus *Col1-Cre* by ANOVA showed $p < 0.05$.

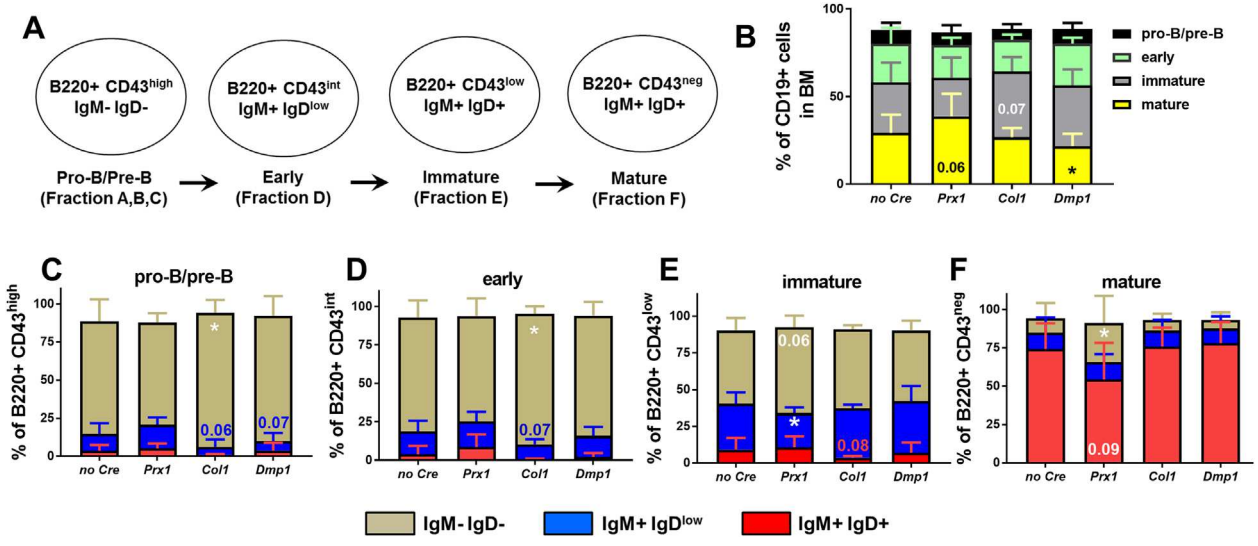

Fig. 4. Loss of Sost in MSCs and OBs differentially regulates earlier and later stages of B cell development in the BM. A) Schematic of B lineage maturation in the BM, with cell surface markers for each maturation stage indicated. B) Stacked bar graph of mean frequencies + standard deviation of progenitor (pro-B/pre-B, black) early (light green), immature (grey) and mature (yellow) B cell stages, and mean frequencies + standard deviation of IgM- IgD- (beige), IgM+ IgD^{low} (blue), and IgM+ IgD+ (red) in C) pro-B/pre-B, D) early, E) immature and F) mature B cells stages in control (no Cre), *Prx1-Cre*, *Col1-Cre*, and *Dmp1-Cre* conditional *Sost* KO mice. $^{*}p < 0.05$, Student's t-test. Exact *p*-values for comparisons of interest that did not achieve $p < 0.05$ are shown in the stacked bar corresponding to the group.

levels of IgM and IgD. Examination of IgM and IgD expression in the mature B cells of the *Sost*$^{iCOIN/iCOIN}$; *Prx1-Cre* BM revealed an abnormally high proportion of cells that lacked expression of both IgM and IgD (Figs. 4*F*, S2*B*). In line with this, the *Sost*$^{iCOIN/iCOIN}$; *Prx1-Cre* mice displayed the lowest proportion of mature IgM+ IgD+ cells among the different mouse strains (Fig. 4*F*). Closer examination of the immature B220+ CD43^{int} subset showed a similar trend of a higher percentage of IgM- IgD- cells and a lower percentage of IgM+ IgD^{low} cells in the *Sost*$^{iCOIN/iCOIN}$; *Prx1-Cre* BM (Fig. 4*E*). These results indicate that deletion of Sost in the *Prx1*+ cells affects the upregulation of IgM and IgD at the later stages of B-cell maturation.

We also observed changes in B-cell maturation in the *Sost*$^{iCOIN/iCOIN}$; *Col1-Cre* BM, but in contrast to the *Prx1-Cre* BM, the progenitor and early stages of development were altered. Significantly higher proportions of IgM- IgD- cells were observed at the B220+ CD43^{high} and B220+ CD43^{int} stages (Fig. 4*C*, 4*D*), as well as a lower proportion IgM+ IgD^{low} cells. This suggests that the progression of B cells from the progenitor to early stages of development was somewhat delayed, and could explain the increased proportion of immature B220+ CD43^{low} cells in the *Sost*$^{iCOIN/iCOIN}$; *Col1-Cre* BM (Fig. 4*B*) and lower percentage and number of IgM+ IgD+ cells within this subset compared to the other mouse strains (Figs. 4*E*, S2*C*, S3*C*). Despite these changes, the proportions and numbers of mature B220+ CD43^{neg} were not similar to Cre controls (Figs. 4*F*, S3D). Results from the analysis of B-cell subsets using alternative staining strategies were consistent with these results (data not shown). B-cell development in *Sost*$^{iCOIN/iCOIN}$; *Dmp1-Cre* BM was not significantly altered at any stage (Fig. 4*C*–*F*). These data suggest that *Prx1-Cre* and *Col1-Cre,* but not *Dmp1-Cre* deletion, remove sclerostin in a subtype of osteoprogenitors required for distinct stages of B-cell development.

ColX-Cre deletion of Sost results in high bone mass

ColX-Cre drives Cre recombinase expression in hypertrophic chondrocytes—cells that recently have been shown to transdifferentiate into osteoblasts.[25,27] Using lineage tracing, it has been shown that *ColX*-positive cells substantially participate in trabecular, endosteal, and cortical bone formation.[26] To determine whether conditional ablation of *Sost* in these cells also affects bone mass, we compared *ColX-Cre* conditional KOs with the Cre-negative littermates. MicroCT analysis of distal femurs showed that *Sost*$^{iCOIN/iCOIN}$; *ColX-Cre* KOs had a significant 37.57% increase in the femoral and a 22.71% increase in the vertebral trabecular bone volume fractions (BV/TV) relative to the Cre negative controls (Table 3). Cortical bone mineral content was slightly elevated, but no other cortical parameters were significantly different, suggesting that *ColX-Cre* ablates *Sost* from a unique population of osteoprogenitor cells that give rise to Sost positive cells in adult bone. LacZ staining of mice carrying a *Sost-LacZ* allele did not detect Sost/LacZ expression in the hypertrophic chondrocytes of neonatal mice (Fig. S4*C*), suggesting that the high bone mass phenotype is due to a subpopulation of *Sost*-deficient osteoblasts and osteocytes, primarily in the trabecular compartment.

Discussion

Sost/sclerostin is highly expressed in the osteocyte population (Fig. S4*A*, *B*); thus it has been hypothesized that the phenotypes observed in bone and hematopoietic development when *Sost* is deleted were due to a lack of *Sost* in the osteocytes. Contrary to this assumption, *Dmp1-Cre* deletion did not recapitulate the global *Sost* phenotype, unlike *Prx1-Cre,* which fully recapitulated the *Sost* global phenotype in the appendicular skeleton. This result can have several interpretations: Either *Dmp1-Cre* is incapable of ablating the *Sost* allele in all *Sost*-expressing osteocytes, and the residual nonrecombined osteocytes express sufficient *Sost* to blunt the otherwise strong phenotype locally, or several distinct populations of cells in the bone express *Sost*, and all these cells are derived from *Prx1*-positive progenitors. The interpretation that other cell types in addition to osteocytes are important contributors to the local pool of sclerostin protein in bone is further supported by the observation that the *Col1-Cre* deletion of *Sost* also had a HBM phenotype, but significant differences were noted between *Col1* and *Dmp1* deletions. For example, a significant difference was observed in the femoral cortical thickness, where *Dmp1* deletion did not increase the cortical thickness, but both *Col1* and *Prx1* did, implying that a subpopulation of periosteal osteoblasts do express *Sost* and these cells could be a population of osteochondral progenitors as previously suggested by Quyang and colleagues.[28]

Because only *Prx1-Cre* deletion of *Sost* recapitulates the HBM phenotype of *Sost* global KO, in the appendicular skeleton, we can conclude that the only *Sost* expression affecting bone mass is derived from descendants of *Prx1*-positive limb bud progenitors (Fig. 5). During the embryonic development of *Prx1*- positive MSCs give rise to muscle, adipocyte, and osteochondral progenitors, which are the predecessors of mature myocytes, adipocytes, chondrocytes, hypertrophic chondrocytes, osteoblasts, and osteocytes. Although endogenous *Prx1* is also expressed in the vertebrae and is required for early events of skeletogenesis in multiple lineages,[29] the *Prx1-Cre* transgene expresses Cre recombinase from a limb enhancer; therefore, the *Cre* expression is restricted to all limb bud MSC derived cells of the appendicular skeleton.[20] Here we showed that *Sost* deletion in mature osteoblasts and their descendant (*Col1-Cre*) or mature osteocytes (*Dmp1-Cre*) elevate bone mass by 80%, respectively, whereas deletion in hypertrophic chondrocytes and their descendants (*ColX-Cre*) elevated trabecular bone mass by 37%. Although all these individual alleles do have a significant HBM phenotype, yet, they do not cumulatively sum up to *Prx1-Cre* or *Sost*$^{-/-}$ alleles (80% + 80% + 37.5% < 250% BV/TV; Tables 1–3), further strengthening the argument that additional *Prx1*-derived cells are responsible for *Sost* expression in bone. The two lineages not represented in our collection of *Cre* alleles are the myogenic and the adipogenic lineages, which cannot yet be excluded as contributors to both the HBM and the B-cell phenotypes. Mining available microarrays and RNA-seq data sets did not identify significant transcript levels of *Sost* in other *Prx-1*-derived cell types; however, future improvements in cell purification methods followed by RNA-seq may identify subpopulations of cell expressing *Sost*. *Sost* expression has also been observed in the osteoclasts of aging mice[30]; although we did not examine the phenotype of osteoclast-specific deletion of *Sost*, neither global *Sost* KO nor any of the conditional strains examined showed a significant change in markers of resorption (Fig. S5).

Herein, we have also presented data that emphasize novel roles for sclerostin in MSCs and OBs, which distinctly impact BM cellularity and B-cell maturation. We conclude that the loss of Sost in mature osteocytes does not play a major role in regulating B-cell development. Loss of *Sost* expression in *Prx1*-positive MSCs and their descendants resulted in reduced BM cellularity, whereas

Table 3. *Sost*$^{iCOIN/iCOIN}$; *ColX*-Cre Bone Phenotyping by microCT

Distal Femur Trabecular and Cortical Compartments			
	ColX-Cre		
Index	Cre− (N = 6)	Cre+ (N = 5)	% change
Trab.TV (mm^3)	2.841 ± 0.315	2.810 ± 0.414	n/c
Trab.BV (mm^3)	0.520 ± 0.138	0.694 ± 0.089*	+33.45
Trab.BV/TV (%)	0.181 ± 0.322	0.249 ± 0.036*	+37.57
Trab.Conn.D. ($1/mm^3$)	125.6 ± 25.08	131.8 ± 20.66	+4.94
Trab.SMI	2.088 ± 0.390	1.296 ± 0.237*	−37.93
Trab.N (1/mm)	4.564 ± 0.317	4.720 ± 0.209	+3.42
Trab.Th (mm)	0.058 ± 0.002	0.064 ± 0.003*	+10.34
Trab.Sp (mm)	0.206 ± 0.017	0.189 ± 0.014	−8.25
Trab.BMC ($\mu gHA/cm^3$)	0.481 ± 0.126	0.643 ± 0.079*	+33.68
Cort.TV (mm^2)	5.918 ± 0.532	6.033 ± 0.608	+1.94
Cort.BV (mm^2)	2.611 ± 0.189	2.788 ± 0.169	+6.78
Cort.BV/TV (%)	0.441 ± 0.056	0.462 ± 0.358	+4.76
Cort. Th (mm)	0.224 ± 0.013	0.224 ± 0.014	0
Cort.BMC ($\mu gHA/cm^3$)	2.806 ± 0.180	3.035 ± 0.154*	+8.16
Cort.BMD ($\mu gHA/cm^3$)	1.075 ± 0.015	1.089 ± 0.016	+1.4
Cancellous (Trabecular) Bone Compartment of the L4 Vertebrae			
	ColX-Cre		
Index	Cre− (N = 5)	Cre+ (N = 5)	% change
Trab.TV (mm^3)	1.736 ± 0.173	1.682 ± 0.119	−3.11
Trab.BV (mm^3)	0.439 ± 0.082	0.515 ± 0.060	+17.31
Trab.BV/TV (%)	0.251 ± 0.026	0.308 ± 0.047*	+22.71
Trab.Conn.D. ($1/mm^3$)	182.81 ± 14.98	194.53 ± 22.06	+6.59
Trab.SMI	0.495 ± 0.300	0.001 ± 0.494	−98.98
Trab.N (1/mm)	4.911 ± 0.189	5.464 ± 0.357*	+11.26
Trab.Th (mm)	0.048 ± 0.003	0.053 ± 0.003	+10.41
Trab.Sp (mm)	0.193 ± 0.007	0.168 ± 0.011*	−12.95
Trab.BMC ($\mu gHA/cm^3$)	0.379 ± 0.078	0.435 ± 0.053	+14.75

Data are from 16-week-old male mice and represent mean ± SD for parameters measured. Trab = trabecular; Cort = cortical; Cort.Th = cortical thickness; BV = bone volume; TV = total volume; Conn.D. = connectivity density; SMI = structural model index; Trab.N = trabecular number; Trab. Th = trabecular thickness; Trab.Sp = trabecular separation; BMC = bone mineral content; BMD = bone mineral density.*p values <0.05; data from 16-week old males.

this process was unaffected by *Sost*-deficiency in mature osteoblasts (*Col1-Cre*) and osteocytes (*Dmp1-Cre*). Furthermore, MSC-specific depletion of *Sost* caused an accumulation of abnormal B cells with no or low expression of IgM and IgD receptors that otherwise appeared phenotypically mature. The changes observed in the frequencies and the absolute numbers of B-cell subsets did not follow the same patterns. For example, the percentage of progenitors and early, immature, and mature B-cell subsets increased or decreased among the different deleter strains, but their numbers were not significantly different among all groups (Figs. 4*B*, S3). This may stem from the fact that MSCs, osteoblasts, and osteocytes have a progenitor–progeny relationship, and it is likely that the deletion of *Sost* in each cell type is not synchronized, so some MSCs may progress to the osteoblast stage before *Sost* deletion occurs and support B-cell development normally. Because total BM cellularity is decreased in the *Prx1-Cre* mice, one might expect that the cell number in all fractions would be proportionally decreased; however, only numbers of B220+ CD43^{int} immature cells were significantly reduced when *Sost* was deleted in MSCs, indicating that immature B cells require normal *Sost* levels. Our findings are consistent with recent work that demonstrated that MSCs and osteoblasts are important "niche cells" for early B-cell development, with respect to their production of CXCL12.[31,32] CXCL12 expression is regulated by Wnt signaling in BM stromal cells in vitro.[33] We observed diminished CXCL12 levels in nonhematopoietic cells of the bone and correlated the diminished CXCL12 levels with the reduction in B-cell development in the global *Sost*$^{-/-}$ mice.[17] Our present results suggest that *Sost* specifically expressed in MSCs and osteoblasts regulate B-cell development, but further analysis is required to determine if expression of CXCL12 and other Wnt target genes are altered in MSCs and osteoblasts in the *Prx1-Cre* and *Col1-Cre Sost* deleters.

Alternatively, it is possible that the B-cell defect is indirect. Recently, we have observed that BM adiposity positively correlates with *Sost* expression levels, such that a mouse model of type I diabetes mellitus with elevated levels of Sost displayed enhanced BM adiposity and this phenotype was rescued by Sost antibody treatment.[19] Also, a recent report has described sclerostin as a promoter of adipogenic differentiation,[34]

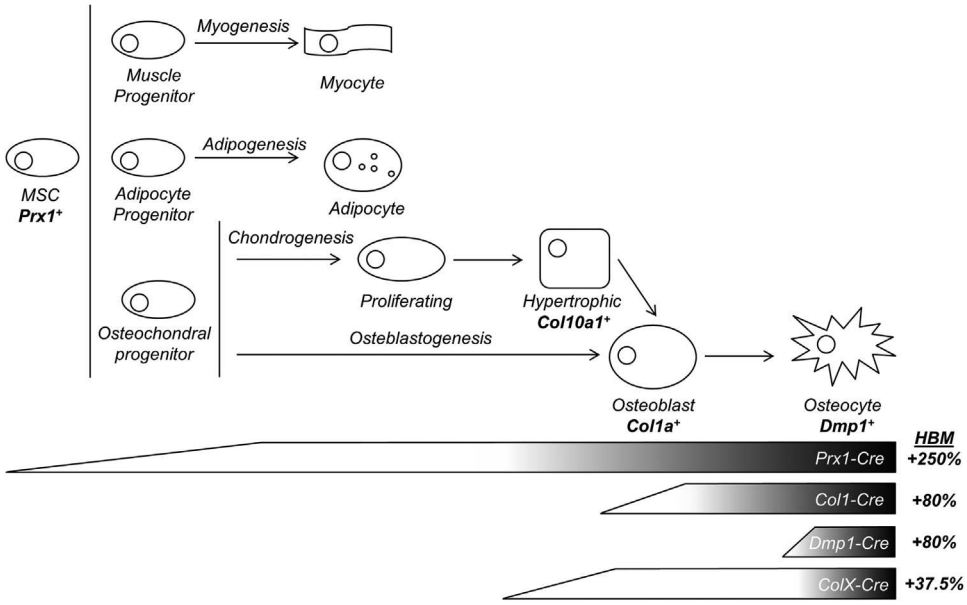

Fig. 5. Cell types along the mesenchymal skin cell/*Prx1-Cre* lineages. *Prx1-Cre* deletes early during differentiation and ablates *Sost* in all derived cells; this mouse fully recapitulates the *Sost*$^{-/-}$ phenotypes. *Col1-Cre* and *Dmp1-Cre* ablate *Sost* in the osteoblast lineage, and both deletions result in similar phenotypes. *ColX-Cre* ablates *Sost* in the hypertrophic chondrocytes, and has the lowest increase in BM. HBM = high bone mass.

suggesting that the lack of Sost may impair adipogenesis. BM adipocytes can be lineage-traced using *Prx1-Cre* and *Osx-Cre*, in contrast to other adipocyte lineages,[35] and the microenvironment in the BM of aged mice appears to favor adipogenesis over osteogenesis in mesenchymal progenitor cells.[36] The relationship between adipocytes and immune cell development is a current area of research. The transition of human common lymphocyte progenitors to the early Pro-B/Pre-B cell stages have been shown to be inhibited by a soluble factor produced by BM adipocytes,[37] and stem cell factor, produced by Lepr+ BM adipocyte precursors, is necessary for the generation of B cells and other hematopoietic cells in mice.[38] Based on these data, any impairment in adipogenesis by Sost depletion may be unrelated to the decrease in mature B cells we have observed in *Sost*-KO mice. Nonetheless, it would worth exploring whether Sost affects B-cell development by interfering with BM adipogenesis. Our analysis of global *Sost* KO mice showed significant decreases in the B-cell precursors and immature subsets, but this was not as dramatic in the *Sost*$^{iCOIN/iCOIN}$; *Prx1-Cre* mice, which suggests that there is another cell that expresses *Sost* that is important in supporting these early B-cell subsets. In contrast, *Prx1*+ and *Col1*+ Sost-expressing cells are critical for normal B-cell maturation. It remains to be determined whether the BM adipocytes in these *Sost*-deficient mice are reduced or impaired in their function to support B-cell maturation.

Our analyses demonstrate that deletion of *Sost* in mature osteocytes does not significantly impair B-lymphocyte development, nor does it cause the HBM observed in the global *Sost*$^{-/-}$; therefore, other cell types derived from *Prx1*-positive MSCs are critical in these processes. Furthermore, we show that *Prx1-Cre* deletion of *Sost* resulted in a significant increase in bone mass in the axial skeleton, where *Sost* alleles remain WT. This result suggests that Sost expressed in the vertebra is diluted out in the circulation, decreasing the net pool of Sost in the axial skeleton and contributing the increased BV/TV in this tissue; however, the vertebra-derived Sost in circulation does not act in an endocrine fashion, leaving the appendicular skeleton unperturbed. These results indicate that Sost primarily acts locally in bone via paracrine secretion and that endocrine secretion of Sost from distant sites does not significantly impair bone mass. Because anti-sclerostin antibodies are likely to become a new therapy to build bone in osteoporosis patients, it is imperative to target these therapies to bone to avoid undesired side-effects in other tissues that may require Sost for their proper function, and to test whether these therapies leave B-cell development unperturbed in these patients. Our results suggest that if Sost-depletion by Sost antibodies is limited to osteocytes, possible side effects on B-cell development and immunity could be avoided, but may elicit a more modest anabolic effect on bone mass.

Disclosures

None.

Acknowledgments

This work was performed under the auspices of the U.S. Department of Energy by Lawrence Livermore National Laboratory under Contract DE-AC52-07NA27344. CSY, JC, NRH, DKM, and GGL were supported in part by NIH Grants RO1 DK075730 and R56 DK110145. JOM was funded by the University of California. We thank the staff in the Department of Animal Research Services at UC Merced and at LLNL for their excellent mouse care.

Authors' roles: GGL and JOM designed the research. CSY, JOM, JC, NRH, JB, MEM and DKM performed the research. AEE generated and provided the *Sost*^{iCOIN} allele. AGR and DJH performed μCT scans and analyses. GGL and JOM analyzed the data. CSY, JOM, and GGL wrote the article.

References

1. Baron R, Kneissel M. WNT signaling in bone homeostasis and disease: from human mutations to treatments. Nat Med. Feb 2013;19-(2):179–92. Epub 2013 Feb 8.
2. Atkins GJ, Rowe PS, Lim HP, Welldon KJ, Ormsby R, Wijenayaka AR, et al. Sclerostin is a locally acting regulator of late-osteoblast/preosteocyte differentiation and regulates mineralization through a MEPE-ASARM-dependent mechanism. J Bone Miner Res. Jul 2011;26(7):1425–36.
3. Balemans W, Ebeling M, Patel N, Van Hul E, Olson P, Dioszegi M, et al. Increased bone density in sclerosteosis is due to the deficiency of a novel secreted protein (SOST). Hum Mol Genet. Mar 2001;10(5):537–43. Epub 2001 Feb 22.
4. Brunkow ME, Gardner JC, Van Ness J, et al. Bone dysplasia sclerosteosis results from loss of the SOST gene product, a novel cystine knot-containing protein. Am J Hum Genet. Mar 2001;68-(3):577–89. Epub 2001 Feb 17.
5. Collette NM, Genetos DC, Economides AN, et al. Targeted deletion of Sost distal enhancer increases bone formation and bone mass. Proc Natl Acad Sci U S A. 2012 Aug 28;109(35):14092–7. Epub 2012 Aug 10. DOI:10.1073/pnas.1207188109.
6. Li X, Ominsky MS, Niu QT, et al. Targeted deletion of the sclerostin gene in mice results in increased bone formation and bone strength. J Bone Miner Res. Jun 2008;23(6):860–9.
7. Loots GG, Kneissel M, Keller H, et al. Genomic deletion of a long-range bone enhancer misregulates sclerostin in Van Buchem disease. Genome Res. Jul 2005;15(7):928–35.
8. Collette NM, Yee CS, Murugesh D, et al. Sost and its paralog Sostdc1 coordinate digit number in a Gli3-dependent manner. Dev Biol. Nov 2013;383(1):90–105.
9. Winkler DG, Sutherland MK, Geoghegan JC, et al. Osteocyte control of bone formation via sclerostin, a novel BMP antagonist. Embo J. Dec 2003;22(23):6267–76. Epub 2003 Nov 25.
10. Jastrzebski S, Kalinowski J, Stolina M, et al. Changes in bone sclerostin levels in mice after ovariectomy vary independently of changes in serum sclerostin levels. J Bone Miner Res. Mar 2013;28(3):618–26. Epub 2012 Oct 10.
11. Ardawi MS, Al-Kadi HA, Rouzi AA, Qari MH. Determinants of serum sclerostin in healthy pre- and postmenopausal women. J Bone Miner Res. Dec 2011;26(12):2812–22. Epub 2011 Aug 4.
12. Mirza FS, Padhi ID, Raisz LG, Lorenzo JA. Serum sclerostin levels negatively correlate with parathyroid hormone levels and free estrogen index in postmenopausal women. J Clin Endocrinol Apr 2010;95(4):1991–7. Epub 2010 Feb 17.
13. Fujita K, Roforth MM, Demaray S, et al. Effects of estrogen on bone mRNA levels of sclerostin and other genes relevant to bone metabolism in postmenopausal women. J Clin Endocrinol Metab. Jan 2014;99(1):E81–8. Epub 2013 Oct 31.
14. Chung YE, Lee SH, Lee SY, et al. Long-term treatment with raloxifene, but not bisphosphonates, reduces circulating sclerostin levels in postmenopausal women. Osteoporos Int. Apr 2012;23(4):1235–43. Epub 2011 June 11.
15. Cain CJ, Rueda R, McLelland B, Collette NM, Loots GG, Manilay JO. Absence of sclerostin adversely affects B cell survival. J Bone Miner Res. 2012 Jul;27(7):1451–61. Epub 2012 Mar 22. DOI:10.1002/jbmr.1608.
16. Economides AN, Frendewey D, Yang P, et al. Conditionals by inversion provide a universal method for the generation of conditional alleles. Proc Natl Acad Sci U S A. Aug 2013;110(34): E3179–88. Epub 2013 Aug 7.
17. Chang JC, Christiansen BA, Murugesh DK, et al. SOST/sclerostin improves post traumatic osteoarthritis and inhibits MMP2/3 expression after injury. J Bone Miner Res. 2018 Jan 26. DOI: 10.1002/jbmr.3397. [Epub ahead of print]
18. Bouxsein ML, Boyd SK, Christiansen BA, Guldberg RE, Jepsen KJ, Muller R. Guidelines for assessment of bone microstructure in rodents using micro-computed tomography. J Bone Miner Res. Jul 2010;25(7):1468–86. Epub 2010 Jun 10.
19. Yee CS, Xie L, Hatsell S, et al. Sclerostin antibody treatment improves fracture outcomes in a Type I diabetic mouse model. Bone. Jan 2016;82:122–34.
20. Logan M, Martin JF, Nagy A, Lobe C, Olson EN, Tabin CJ. Expression of Cre recombinase in the developing mouse limb bud driven by a Prxl enhancer. Genesis. Jun 2002;33(2):77–80. Epub 2002 July 12.
21. Liu F, Woitge HW, Braut A, et al. Expression and activity of osteoblast-targeted Cre recombinase transgenes in murine skeletal tissues. Int J Dev Biol. Sep 2004;48(7):645–53. Epub 2004 Oct 8.
22. Lu Y, Xie Y, Zhang S, Dusevich V, Bonewald LF, Feng JQ. DMP1-targeted Cre expression in odontoblasts and osteocytes. J Dent Res. Apr 2007;86(4):320–5. Epub 2007 Mar 27.
23. van Bezooijen RL, ten Dijke P, Papapoulos SE, Lowik CW. SOST/sclerostin, an osteocyte-derived negative regulator of bone formation. Cytokine Growth Factor Rev. Jun 2005;16(3):319–27. Epub 2005 May 5.
24. Hardy RR, Carmack CE, Shinton SA, Kemp JD, Hayakawa K. Resolution and characterization of pro-B and pre-pro-B cell stages in normal mouse bone marrow. J Exp Med. May 1991 173(5): 1213–25.
25. Khass M, Buckley K, Kapoor P, et al. Recirculating bone marrow B cells in C57BL/6 mice are more tolerant of highly hydrophobic and highly charged CDR-H3s than those in BALB/c mice. Eur J Immunol. Mar 2013;43(3):629–40. Epub 2012 Dec 12.
26. Park J, Gebhardt M, Golovchenko S, et al. Dual pathways to endochondral osteoblasts: a novel chondrocyte-derived osteoprogenitor cell identified in hypertrophic cartilage. Biol Open. Apr 2015;4(5):608–21.
27. Yang L, Tsang KY, Tang HC, Chan D, Cheah KS. Hypertrophic chondrocytes can become osteoblasts and osteocytes in endochondral bone formation. Proc Natl Acad Sci U S A. Aug 2014;111(33):12097–102.
28. Ouyang Z, Chen Z, Ishikawa M, et al. Prx1 and 3.2kb Col1a1 promoters target distinct bone cell populations in transgenic mice. Bone. 2013 Oct 25. pii: S8756–3282(13) 00426–2. DOI: 10.1016/j.bone.2013.10.016
29. Martin JF, Bradley A, Olson EN. The paired-like homeo box gene MHox is required for early events of skeletogenesis in multiple lineages. Genes Dev. May 1995;9(10):1237–49. Epub 1995 May 15.
30. Ota K, Quint P, Ruan M, et al. Sclerostin is expressed in osteoclasts from aged mice and reduces osteoclast-mediated stimulation of mineralization. J Cell Biochem. Aug 2013;114(8):1901–7. Epub 2013 Mar 16.
31. Ding L, Morrison SJ. Haematopoietic stem cells and early lymphoid progenitors occupy distinct bone marrow niches. Nature. Mar 2013;495(7440):231–5. Epub 2013 Feb 26.
32. Nagasawa T. The chemokine CXCL12 and regulation of HSC and B lymphocyte development in the bone marrow niche. Adv Exp Med Biol. 2007;602:69–75.
33. Tamura M, Sato MM, Nashimoto M. Regulation of CXCL12 expression by canonical Wnt signaling in bone marrow stromal cells. Int J Biochem Cell Biol. May 2011;43(5):760–7. Epub 2011 Feb 8.
34. Ukita M, Yamaguchi T, Ohata N, Tamura M. Sclerostin enhances adipocyte differentiation in 3T3-L1 cells. J Cell Biochem. Jun 2016;117(6):1419–28.
35. Horowitz MC, Berry R, Holtrup B, et al. Bone marrow adipocytes. Adipocyte. 2017 Jul 3;6(3):193–204. Epub 2017 Aug 24. DOI:10.1080/21623945.2017.1367881.
36. Singh L, Brennan TA, Russell E, et al. Aging alters bone-fat reciprocity by shifting in vivo mesenchymal precursor cell fate towards an adipogenic lineage. Bone. Apr 2016;85:29–36.
37. Bilwani FA, Knight KL. Adipocyte-derived soluble factor(s) inhibits early stages of B lymphopoiesis. J Immunol. Nov 2012;189(9): 4379–86.
38. Zhou BO, Yu H, Yue R, et al. Bone marrow adipocytes promote the regeneration of stem cells and haematopoiesis by secreting SCF. Nat Cell Biol. Aug 2017;19(8):891–903.